Antifungal polycyclic tetramate macrolactam HSAF is a novel oxidative stress modulator in *Lysobacter enzymogenes*

Running title: HSAF as a novel oxidative stress modulator

Lingjun Yu,[1,2] Hui Li,[2,3] Zaichun Zhou,[2,4] Fengquan Liu[1*] and Liangcheng Du[2*]

[1] *Institute of Plant Protection, Jiangsu Academy of Agricultural Sciences, Nanjing, 210014, China*

[2] *Departments of Chemistry, University of Nebraska-Lincoln, NE 68588, USA*

[3] *Nebraska Center for Materials and Nanoscience and Center for Integrated Biomolecular Communication, University of Nebraska-Lincoln, NE 68588, USA*

[4] *Key Laboratory of Theoretical Organic Chemistry and Functional Molecules, Ministry of Education; School of Chemistry and Chemical Engineering, Hunan University of Science and Technology, Xiangtan 411201, China*

*For corresponding: Liangcheng Du, Departments of Chemistry, University of Nebraska-Lincoln, NE 68588, USA. E-mail: ldu3@unl.edu, Phone: 1-402-472-2998.

Fengquan Liu, Institute of Plant Protection, Jiangsu Academy of Agricultural Sciences, Nanjing, 210014, China. E-mail: fqliu20011@sina.com.

ABSTRACT

Polycyclic tetramate macrolactams (PoTeM) are a fast-growing family of antibiotic natural products found in phylogenetically diverse microorganisms. Surprisingly, none of the PoTeM had been investigated for potential physiological functions in their producers. Here, we used HSAF (heat-stable antifungal factor), an antifungal PoTeM from *Lysobacter enzymogenes*, as a model to show that PoTeM forms complexes with iron ion, with a K_a of $2.71*10^6$. The *in vivo* and *in vitro* data showed formation of 2:1 and 3:1 complexes between HSAF and iron ions, which were confirmed by molecular mechanical and quantum mechanical calculations. HSAF protected DNA from degradation in high concentrations of iron and H_2O_2 or under UV radiation. HSAF mutants of *L. enzymogenes* barely survived under oxidative stresses and markedly increased the production of reactive oxygen species (ROS). Exogenous addition of HSAF into the mutants significantly prevented ROS production and rescued the mutants to normal growth under the oxidative stresses. The results reveal that the function of HSAF is to protect the producer microorganism from oxidative damages, rather than as an iron-acquisition siderophore. The characteristic structure of PoTeM, 2,4-pyrrolidinedione-embedded macrolactam, may represent a new iron-chelating scaffold of microbial metabolites. Together, the study demonstrated a previously unrecognized strategy for microorganisms to modulate oxidative damages to the cells.

44 **Importance**

45 Polycyclic tetramate macrolactams (PoTeM) are a family of structurally distinct metabolites
46 that have been found in a large number of bacteria. Although PoTeM exhibit diverse
47 therapeutic properties, the physiological function of PoTeM in the producer microorganisms
48 had not been investigated. HSAF from *Lysobacter enzymogenes* is an antifungal PoTeM that
49 has been subjected to extensive studies for mechanism of biosynthesis, regulation and the
50 antifungal activity. Using HSAF as a model system, we here showed that the characteristic
51 structure of PoTeM, 2,4-pyrrolidinedione-embedded macrolactam, may represent a new
52 iron-chelating scaffold of microbial metabolites. In *L. enzymogenes*, HSAF functions as a
53 small molecule modulator for oxidative damages caused by iron, H_2O_2 and UV light.
54 Together, the study demonstrated a previously unrecognized strategy for microorganisms to
55 modulate oxidative damages to the cells. HSAF represents the first member of the fast
56 growing PoTeM family of microbial metabolites whose potential biological function has been
57 studied.

58

59 **Key Words:** natural products, polycyclic tetramate macrolactams, *Lysobacter enzymogenes*,
60 oxidative damage, iron binding

61

62

63 **Introduction**

64

65 Polycyclic tetramate macrolactams (PoTeM) are a family of natural products with diverse
66 therapeutic properties, including antibacterial, antifungal, anti-protozoa, and anticancer (1-9).
67 Their structures share a characteristic 2,4-pyrrolidinedione (tetramate)-containing
68 macrolactam and have been found in phylogenetically diverse bacteria. For example,
69 ikarugamycin, frontalamides, clifednamides, pactamides, capsimycins, and carbamides were
70 isolated from various species of *Streptomyces* (1, 3-5, 8-10). HSAF and several alteramides
71 were reported from several *Lysobacter* strains (2, 11-15). Maltophilin and xanthobaccin were
72 isolated from *Stenotrophomonas* strains (16, 17). Discodermide and cylindramide were from
73 marine sponges (18, 19). Umezawamides were from a combined-culture of *Umezawaea* sp.
74 and mycolic-acid containing bacterium *Tsukamurella pulmonis* (20).

75 The biosynthetic gene cluster (BGC) for several PoTeM have been reported (2, 3, 5,
76 10-14). Although the chemical structures are complex, the BGC exhibits a relative simplicity
77 and a conserved organization. In the center of the BGC is always a single-module PKS-NRPS
78 hybrid gene, which is sufficient to construct the scaffold of PoTeM (10-12, 14, 21-23).
79 Flanking the PKS-NRPS gene are 2-6 accessory genes, which are responsible for the
80 structural diversity of PoTeM (14). Cryptic BGCs with this unique organization are present in
81 numerous genome sequences in the databases, implying that there is an immense reservoir of
82 PoTeM type of natural products yet to be discovered from the vast number of microorganisms
83 (3, 9, 10). The therapeutic properties, structural novelty, diverse bioactivities, and distinct
84 biosynthetic mechanism have attracted a lot of research interests in the recent years. However,

essentially nothing is known about PoTeM's physiological functions in their producer organisms.

Many antibiotic metabolites are produced by microorganisms inhabiting in diverse environments. In their native environments, the metabolites are typically not to function as antibiotics to kill or inhibit other microorganisms because the producers rarely produce inhibitory concentrations of the metabolites in the environments (24). Many factors in the environments could affect the metabolite production and stress response in microorganisms. For example, reactive oxygen species (ROS) are stimulated in microorganisms when growing in a high iron environment or other stressed environments. Bacteria have evolved several strategies to modulate the oxidative stress induced by a high ROS level. The thioredoxin (Trx) system (NADPH, thioredoxin reductase and thioredoxin) is a crucial antioxidant system in bacteria. The system removes ROS through providing electrons to thiol-dependent peroxidases. In most Gram-negative bacteria, glutaredoxin system (Grx) and catalase provide a strong backup for the Trx system (25). Some catalase-negative bacteria such as *Streptococcus pyogenes* mainly utilize the thiol-dependent peroxidase system in defense against oxidative stress although both Trx and Grx exist (26). Besides, carotenoids and the aryl polyene type bacterial pigments are proved to protect bacteria from ROS, which is related to their conjugation double bond systems (27-29). Recently, the H_2S-mediated mechanism was found in protection against oxidative stress in *Escherichia coli* (30). The endogenous H_2S produced by 3-mercaptopyruvate sulfurtransferase sequestrates free ion, which is necessary for the genotoxic Fenton reaction (30).

In this study, we have used the small molecule metabolite, HSAF (heat-stable antifungal

107 factor), from *L. enzymogenes,* as a model PoTeM to explore its potential physiological
108 functions. HSAF and alteramides (Fig. 1) isolated from *L. enzymogenes* are arguably the most
109 extensively investigated PoTeM in terms of structural diversity, bioactivities and modes of
110 action, and molecular mechanisms for biosynthesis (2, 6, 7, 11-14, 31). Here, our results
111 showed that the characteristic structure of PoTeM, 2,4-pyrrolidinedione-embedded
112 macrolactam, can act as a new iron-chelating natural product scaffold. HSAF functions as a
113 small molecule modulator for oxidative damages caused by iron, H_2O_2 and UV light in *L.*
114 *enzymogenes*. Together, the study demonstrated a previously unrecognized strategy for
115 microorganisms to modulate oxidative damages to the cells.
116

117 **RESULTS**

118 *Formation of brown-orange complexes between HSAF and iron*

119 During the study of *L. enzymogenes* OH11, we serendipitously found that adding iron salts
120 into minimal culture media could make OH11 grow more robustly (Fig. S1a). When we
121 investigated the effect of different concentrations of $FeSO_4$ (0, 1, 10, 100 and 500 μM) on the
122 growth of OH11 in a modified minimal medium (M813m) (Figure S1b), we observed
123 formation of brown-orange substances in both the cultures and the HSAF extracts (Fig. 2a-b).
124 This color was intensified with the increase of the $FeSO_4$ concentration and was absent in the
125 culture or extracts from HSAF mutant (ΔHSAF) (32), even when grown in M813m
126 containing 500 μM $FeSO_4$. The result suggested that HSAF and iron ions might be able to
127 interact with one another and form certain pigment complexes in the culture of OH11.
128 Moreover, we found $FeSO_4$ could significantly boost the production of HSAF and alteramides

(Fig. S2). With 1-10 μM $FeSO_4$ in M813m, the amount of free HSAF increased about 10-14 folds, compared to the medium without $FeSO_4$.

To verify the HSAF-iron complexes, we extracted the total PoTeM mixture, containing both HSAF and its analogs (alteramides), from the cultures. When the mixture was added into an aqueous solution of $FeSO_4$, the solution turned to the brown-orange color, with a gradually increased intensity following the increase of the PoTeM mixture, while the controls remained colorless (Fig. 2c). Furthermore, the same color could be developed in the PoTeM mixture when added with other iron salts, such as $Fe(NH_4)_2(SO_4)_2$, $FeCl_3$ and $Fe(NO_3)_3$ (Fig. 2d). HPLC analysis of the mixtures showed that the PoTeM peaks significantly decreased or disappeared when any of the iron salts was added to the solutions (Fig. 2e). The interaction between PoTeM and iron ions appeared to be specific, because HPLC showed that the PoTeM peaks remained in the solutions, if the mixture was added with other metal ions (Na^+, Mg^{2+}, K^+, Ca^{2+}, Zn^{2+}), although there might have been some interactions between PoTeMs and Cu^{2+} (Fig. S3).

Mass spectrometry of HSAF-Fe complexes

The above observations indicated that HSAF and its analogs could form complexes with iron ions. To obtain direct evidence, we purified HSAF from the OH11 culture and treated HSAF (10 mM) with the same concentration of aqueous $FeSO_4$, $Fe(NH_4)_2(SO_4)_2$, $FeCl_3$, or $Fe(NO_3)_3$. The products were analyzed by mass spectrometry (MS). Without the iron ion, all MS gave two main peaks, *m/z* 513 for $[HSAF+H]^+$ and *m/z* 1025 for $[2HSAF+H]^+$), which are expected for standard HSAF (Fig. 3). Upon treatment with the iron ion, the HSAF peaks

151 markedly decreased (when added with ferrous ion, $FeSO_4$ or $Fe(NH_4)_2(SO_4)_2$) or disappeared
152 (when added with ferric ion, $FeCl_3$ or $Fe(NO_3)_3$). Meantime, two new peaks appeared (*m/z*
153 1079 and 1591) when treated with $FeSO_4$ or $Fe(NH_4)_2(SO_4)_2$ (Fig. 3a-b), or just one new peak
154 appeared (*m/z* 1079) when treated with $FeCl_3$ or $Fe(NO_3)_3$ (Fig. 3c-d). The peak at *m/z* 1079
155 is coincident with $[2HSAF-H+Fe]^+$, whereas the peak at *m/z* 1591 is coincident with
156 $[3HSAF-H+Fe]^+$. The data showed that two or three HSAF molecules could coordinate with
157 one iron ion, to form stable HSAF-Fe complexes that displayed the observed orange-brown
158 color. The data also suggested that all HSAF chelated with Fe when a ferric salt was used, as
159 seen in $FeCl_3$ and $Fe(NO_3)_3$, but only a portion of HSAF chelated with iron when a ferrous
160 salt was used, as seen in $FeSO_4$ and $Fe(NH_4)_2(SO_4)_2$ (Fig. 3). Since ferrous iron can gradually
161 be oxidized to ferric ion in the atmosphere, it is likely that the observed partial chelation in
162 $FeSO_4$ and $Fe(NH_4)_2(SO_4)_2$ was due to the oxidized iron (ferric). Besides, both 2HSAF-Fe
163 and 3HSAF-Fe were observed when ferrous salts were used, whereas only 2HSAF-Fe was
164 detected when ferric salts were used. This also supports that ferric ion is the preferred iron for
165 HSAF chelation, because the concentration of ferric ion in solution would be lower when
166 $FeSO_4$ and $Fe(NH_4)_2(SO_4)_2$ were used than that when $FeCl_3$ and $Fe(NO_3)_3$ were used, and thus
167 HSAF concentration was relatively high and two or three HSAF molecules were available to
168 chelate one ferric ion in $FeSO_4$ and $Fe(NH_4)_2(SO_4)_2$ solutions. To further confirm the
169 formation of HSAF-Fe complexes, EDTA, a strong chelator for metal ions, was added into
170 the mixtures of HSAF and iron salts. MS clearly showed that the HSAF-Fe complexes (*m/z*
171 1079 and 1591) were abolished and HSAF (*m/z* 513 and 1025) was restored (Fig. 3).
172

Absorbance spectra of HSAF-Fe complexes

Next, we analyzed the absorbance spectra of the HSAF-Fe complexes (Fig. S4). Standard HSAF gave a maximum peak at ~323 nm, which shifted to ~310 nm upon addition of any of the iron salts, $FeSO_4$, $Fe(NH_4)_2(SO_4)_2$, $FeCl_3$, or $Fe(NO_3)_3$. While HSAF or the iron salts barely had any absorption in the visible range, the HSAF-Fe complexes gave clear absorptions at ~410-600 nm, which apparently contributed to the orange-brown appearance of the mixtures. Furthermore, the maximal absorption shifted back to 323 nm from 310 nm and the absorption at ~410-600 nm disappeared, upon addition of EDTA (Fig. S4). The absorption spectroscopic data are in accordance with that of MS analysis. Using the UV-visible titration of HSAF with $Fe(NO_3)_3$ and nonlinear curve-fitting at 470 nm, we obtained the association constant (K_a) of HSAF-Fe to be $2.71*10^6$ (Fig. S5). The K_a value is much smaller than that for recognized siderophores (33), indicating that, rather than function as a siderophore for iron acquisition from the environment, HSAF in *L. enzymogenes* may play a new function during the interaction with iron ion.

Antioxidant activity of HSAF and protection of DNA degradation in vitro

To understand possible roles of HSAF in *L. enzymogenes*, we explored the potential involvement of HSAF in modulation of oxidative stress, because it is well known that the cellular iron could generate reactive oxygen species (ROS) due to the Fenton reaction, which can lead to cell death (34). The *in vivo* and *in vitro* data described above showed the formation of HSAF-Fe complexes, which might contribute to maintaining a proper free iron concentration important to redox homeostasis of the bacterial cells.

195 To test this hypothesis, we used the deoxyribose degradation assay to determine HSAF's
196 antioxidant activity (35). HSAF showed a dose-dependent antioxidant activity and behaved as
197 a strong antioxidant when the concentration reached 80-160 μM (Fig. 4a). The reaction
198 system for the assay contained deoxy-D-ribose, H_2O_2, Fe^{3+}, ascorbic acid, and purified HSAF.
199 To exclude possible direct interactions between HSAF and H_2O_2, ascorbic acid, or
200 deoxy-D-ribose, we analyzed the mixtures using HPLC. As expected, HSAF was not affected
201 by any of the factors (H_2O_2, ascorbic acid, deoxy-D-ribose) (Fig. S6). The results indicated
202 that the antioxidant activity of HSAF resulted from the chelation with iron ion. To confirm
203 the antioxidant function of HSAF, we carried out *in vitro* DNA fragment degradation caused
204 by Fenton reaction due to production of the radical species (36). A DNA fragment with the
205 length of 1 Kb was amplified by PCR using the genome of *L. enzymogenes* as template. The
206 DNA fragment was completely degraded in the presence of Fe^{3+} and H_2O_2, while the DNA
207 fragment remained intact in the controls. However, the addition of purified HSAF inhibited
208 the DNA degradation, in a dose-dependent manner (Fig. 4b). When HSAF reached to 80 μM,
209 the DNA fragment was fully protected from the Fenton reaction-caused degradation, which is
210 in good agreement with the antioxidative activity assay (Fig. 4a). To learn whether this
211 protective effect of HSAF is specific to certain DNA fragments, we tested similar length
212 DNA fragments from *Lysobacter* 3655, *Lysobacter antibioticus* OH13, and *Escherichia coli*.
213 HSAF exhibited the similar protective effect against the Fenton reaction-caused damage on
214 these DNA fragments, showing a general antioxidative effect of HSAF (Fig. S7).
215
216 *Protection of L. enzymogenes OH11 from high H_2O_2 stress by HSAF in vivo*

217 The observation that HSAF can protect *in vitro* DNA degradation by H_2O_2 inspired us to
218 investigate HSAF's function *in vivo*. The WT and ΔHSAF strains were treated with different
219 concentrations of H_2O_2 in M813m medium. The results clearly showed that the growth rate of
220 the WT and ΔHSAF was similar when culture medium contained a low concentration of H_2O_2
221 (80 μM), but in the medium containing a high concentration of H_2O_2 (800 μM), the growth
222 rate of ΔHSAF strain significantly decreased when compared to that of the WT (Fig. 4c-4e).
223 Actually, ΔHSAF strain did not grow in M813m containing 800 μM H_2O_2 in the first 48 h and
224 started a slow growth only at 72 h, while the WT grown in M813m containing 800 μM H_2O_2
225 could reach the similar OD_{600} values as the WT without H_2O_2 at 72-96 h. We also analyzed
226 the HSAF level in cultures containing 0, 80 and 800 μM H_2O_2. It showed that the production
227 of HSAF/alteramides in the WT with 800 μM H_2O_2 decreased by 30% when compared to that
228 of the WT with 0 or 80 μM H_2O_2, implying a consumption of HSAF for formation of
229 HSAF-Fe complexes, to protect the cells grown in a high concentration of H_2O_2 (Fig. S8). To
230 exclude the possibility that HSAF in WT could directly degrade H_2O_2 so that WT could grow
231 in a high concentration of H_2O_2, we tested the ability of HSAF and HSAF-Fe complexes to
232 degrade H_2O_2 *in vitro* (Fig. S9). The results show that H_2O_2 was not degraded by either
233 HSAF or HSAF-Fe complexes. Furthermore, MS analysis of the ethyl acetate extract from
234 the WT culture clearly detected the peaks at *m/z* 1079 for $[2HSAF\text{-}H+Fe]^+$ and 1591 for
235 $[3HSAF\text{-}H+Fe]^+$, in addition to *m/z* 513 for $[HSAF+H]^+$ (Fig. S10). This showed HSAF-Fe
236 complexes were formed in vivo.

237

238 *Protection of L. enzymogenes OH11 from high iron stress in vivo*

239 Next, we looked into the effect of HSAF on the growth yield of *L. enzymogenes* OH11 under
240 different concentrations of iron ion. The WT and ΔHSAF strains in regular M813m medium
241 containing 10 μM iron ion exhibited a similar growth yield to that in M813m medium
242 without iron ion (Fig. S11a-b). However, in M813m containing a high concentration (500 μM)
243 of iron ion, the growth yield of ΔHSAF strain was significantly lower than that of the WT
244 after 72-120 h growth, although both strains exhibited a similar growth yield in the first 48 h
245 (Fig. S11c). The addition of HSAF to the cultures after 48 h growth restored the growth yield
246 of ΔHSAF strain to the WT level in the following 72-120 h growth, even when the iron
247 concentration was as high as 500 μM (Fig. S11d). The results show that HSAF can protect
248 OH11 cells from high iron stress *in vivo*. Besides, the exogenously added HSAF-Fe
249 complexes, but not HSAF alone, could promote the growth of WT strain in M813m medium
250 without supplemented $FeSO_4$ (Fig. S12a). However, neither HSAF nor HSAF-Fe complexes
251 affect the growth of WT strain in regular M813m medium containing $FeSO_4$ (Fig. S12b). The
252 results suggested that iron ion could be released from HSAF-Fe complexes and then up-taken
253 by the cells to support the observed growth promotion.
254
255 *Protection of L. enzymogenes OH11 from UV radiation by HSAF*
256 In light of HSAF's protection of *L. enzymogenes* from oxidative damages induced by high
257 concentrations of iron and H_2O_2, we looked into the protective role of HSAF when the cells
258 were exposed to UV radiation, because UV exposure can also lead to a variety of ROS
259 through various mechanisms (37). When the WT and ΔHSAF strains were exposed to the UV
260 light for a short time (10 s), the survival rates of the WT and ΔHSAF cells were similar.

261 However, the survival rate of ΔHSAF cells was significantly decreased when the UV
262 exposure time increased to 30 s, and there was nearly zero colony on the plate with 60 s of
263 UV exposure, while the WT still had a large number of colonies (Fig. 5a, S13a). On the other
264 hand, the exogenous addition of purified HSAF to the ΔHSAF culture before the UV
265 exposure could restore the growth. The rescue of the ΔHSAF cells by HSAF showed a clear
266 dose-dependent manner, and when the HSAF concentration reached 160 μM, the survival rate
267 of ΔHSAF was even higher than that of the WT (Fig. 5b, S12b). The results unequivocally
268 showed the protective effect of HSAF on cells with UV radiation.

269

270 *Repression of ROS accumulation in L. enzymogenes OH11 by HSAF*

271 Next, we tested the ROS formation in the strains using the method of H2DCFDA
272 (2',7'-dichlorodihydrofluorescein diacetate), which is a cell-permeant indicator that generates
273 fluorescence after oxidation by ROS (38). The results showed almost no detectable ROS in
274 the WT and ΔHSAF strains when cultured in the minimal medium without iron ion, and a low
275 level of ROS production similarly in the WT and ΔHSAF strains in the modified medium
276 containing a low level of iron (M813m containing 10 μM $FeSO_4$) (Fig. 5c). In a high iron
277 medium (M813m containing 500 μM $FeSO_4$), ΔHSAF strain produced nearly a double
278 amount of ROS than the WT, although the ROS level increased significantly in both the WT
279 and ΔHSAF. Remarkably, when exogenous HSAF was added to the ΔHSAF strain grown in
280 the 500 μM $FeSO_4$ medium, the ROS level returned to the WT level. The results clearly
281 showed that HSAF is able to repress the high iron-caused ROS production (Fig. 5c).
282 Moreover, the ROS level in ΔHSAF was about 2 fold higher than that in the WT, when

283 treated with H_2O_2 or UV lights, and the exogenous HSAF restored the WT level of ROS in
284 ΔHSAF strain (Fig. 5d-e). Next, we directly measured the ROS scavenging activity of HSAF
285 and HSAF-Fe complexes using DPPH (2,2-Diphenyl-1-picrylhydrazyl), which is a stable
286 radical and has the maximum absorption at 520 nm. The results showed that HSAF and
287 HSAF-Fe complexes exhibited low ROS scavenging activity when the incubation time was
288 0.5 h, while with the extension of incubation time (24 h, 72 h and 120 h), the ROS
289 scavenging activity of both HSAF and HSAF-Fe complexes increased (Fig. S14a-b). As
290 expected, ascorbic acid showed strong ROS scavenging activity (Fig. S14c). This is
291 consistent with the observation in the UV irradiation assay, where the cultural time was 72 h
292 and HSAF exhibited ROS scavenging activity. The data clearly showed the ROS modulating
293 ability of HSAF in *L. enzymogenes*.
294
295 *Molecular structure of HSAF-Fe complexes*
296 To obtain further evidence for formation of the HSAF-Fe complexes, we performed
297 molecular mechanical and quantum mechanical calculations to determine the possible
298 molecular structures of the HSAF-Fe complexes. Using a molecular mechanical force field
299 method, a global search suggested that both Fe^{3+} and Fe^{2+} ions can be chelated by 2 or 3
300 HSAF neutral molecules. Quantum mechanical method was used to refine the molecular
301 geometries (Fig. 6). When 2 molecules of HSAF bind to an iron ion, the 3 carbonyl oxygen
302 atoms (at C7, C25, C27, see Fig. 1) of each of the two HSAF molecules form 3 coordinate
303 bonds to the iron. When 3 molecules of HSAF bind to an iron ion, two HSAF molecues
304 provide the oxygen atoms at C7 and C27, and the third HSAF molecule provides the oxygen

atoms at C25 and C27. Together, the three HSAF molecues form 6 coordinate bonds to the iron. Due to steric factors, it would be impossible for 4 molecules of HSAF to bind to one iron. The carbonyl oxygen atoms at C7, C25 and C27 are absolutely conserved in all PoTeMs, suggesting that formation of such iron complexes are general for all PoTeMs. The chelation status is similar to that of *Pseudomonas* quinolone signal (PQS) with iron ion, in which two or three PQS molecules chelated one iron ion (39).

DISCUSSION

Since the isolation of HSAF and its analogs from *Lysobacter enzymogenes*, the research has focused on their antifungal activity, as well as the molecular mechanism for their biosynthesis and regulation. The work presented here is the first attempt to address the role of these complex molecules in their producer organism. *Lysobacter* species are emerging as a rich source of bioactive natural products. During our efforts to activate silent biosynthetic gene clusters in the genomes of *Lysobacter* species, we serendipitously found that the addition of iron salts enhanced HSAF production. Meantime, we observed the formation of a brown-orange color when iron salts were added to the cultures that produced HSAF and analogs, but not in the biosynthetic mutant. *In vitro* studies using the crude extracts and purified HSAF confirmed that the color was due to formation of complexes between these compounds and iron. The results also showed that the production of HSAF and analogs is essential for *L. enzymogenes* to survive under oxidative conditions that are known to generate reactive oxygen species (ROS).

When *L. enzymogenes* was exposed to a high concentration of iron, H_2O_2, or UV

radiation, the HSAF biosynthetic mutant was barely able to survive, while the wild type and the mutant supplemented with HSAF exogenously could grow normally. In bacteria, ROS are induced by many stresses including presence of a high iron concentration, H_2O_2 treatment, and UV radiation (40). Indeed, we observed a significantly higher level of ROS production in the HSAF mutant than in the wild type. The supplement of HSAF into the mutant reduced the ROS level to that of the wild type.

We also observed that HSAF protects DNA from degradation in the presence of iron and H_2O_2, probably due to hydroxyl radical (·OH), generated by Fenton reaction [Eq. (1)]. Hydroxyl radical is highly reactive ROS and able to oxidize practically every molecule in the cell (41, 42).

$$H_2O_2 + Fe^{2+} \rightarrow {}^{-}OH + {\bullet}OH + Fe^{3+} \qquad (1)$$

In both prokaryotes and eukaryotes, the oxidative DNA damage caused by hydroxyl radical is the primary cause of cell death under oxidative stress conditions (43-45). We thus hypothesized that HSAF may be involved in Fenton reaction and affect the redox homeostasis of *L. enzymogenes*. In bacteria, both $O_2{\bullet}^{-}$ and H_2O_2 are primarily produced by the accidental autoxidation of non-respiratory flavoproteins which are univalent electron donors giving electrons to oxygen (46). Besides, a high iron concentration also could promote the H_2O_2 generation. In deoxyribose degradation assay, ascorbic acid initializes the Fenton reaction by reducing Fe^{3+} to Fe^{2+}, and Fe^{2+} in turn reacts with H_2O_2 to generate ROS (•OH) [Eq. (1)] (35). In the *in vitro* assay of DNA fragment degradation, Fe^{3+} could be reduced to Fe^{2+} through reacting with H_2O_2, by following the two-step reactions [Eq. (2)-(3)] (47). The reactions generate Fe^{2+} and then ROS by the reaction between Fe^{2+} and H_2O_2 as shown in Eq.

(1).

$$H_2O_2 + Fe^{3+} \rightarrow Fe\text{-}OOH^{2+} + H^+ \quad (2)$$

$$Fe\text{-}OOH^{2+} \rightarrow HO_2^{\cdot} + Fe^{2+} \quad (3)$$

As shown in Fig. 2, HSAF prefers ferric ion over ferrous ion in the chelation. The HSAF-Fe^{3+} chelation would prevent the reduction of Fe^{3+} to Fe^{2+} in the two-step reactions [Eq. (2)-(3)]. Consequently, the sequestration of Fe^{3+} ion by HSAF would result in a reduced amount of free Fe^{2+} in the cells and in turn a reduced ROS from the Fenton reaction. The K_a value of HSAF-Fe complexes is significantly smaller than that of typical siderophores. This suggests that a relatively high concentration (μM level) of HSAF would be needed in order to form stable complexes with iron. HSAF and alteramides are the predominant secondary metabolites in *L. Enzymogenes* (2). We were able to obtain up to 50 mg HSAF from 1 L culture, suggesting that the concentration of HSAF in the cells would be higher than 100 μM. Thus, the concentration at which HSAF exhibited iron-chelation and strong antioxidant activity *in vitro* could be readily achievable *in vivo*.

Moreover, we showed that the exogenous addition of HSAF into the culture media could restore the ΔHSAF mutant's growth under high iron concentrations, H_2O_2, and UV radiation; we also showed that the exogenous HSAF was able to make the ROS level in the ΔHSAF mutant return to the WT level, even when grown in the 500 μM $FeSO_4$ medium. Together, these observations implied that extracellular HSAF was able to enter the cells. However, the exact mechanism of HSAF transportation is not totally clear at the moment. Beyond chelating iron, HSAF can also scavenge ROS directly as seen in Fig. 5c-e and Fig. S14a-b. These explain the protective effect of HSAF on *Lysobacter* with UV exposure (Fig. 5a-b).

371 Although HSAF is able to chelate iron, the HSAF-Fe complexes form only when the iron
372 concentration is sufficiently high (above μM level). This is in contrast to siderophores whose
373 primary function is to grab metal ions from the environments where the concentration of the
374 metals can be extremely low. HSAF functions as a modulator for oxidative stresses only
375 when the cells are exposed to an environment with a high concentration of iron, H_2O_2, or
376 exposed to UV light, all of which can lead to ROS generation that damages DNA and cell
377 survival.

378 Moreover, our study using methods in molecular mechanical force field and quantum
379 mechanical indicated that the carbonyl groups at C7, C25 and C27 of HSAF structure are
380 involved in formation of the HSAF-Fe complexes. These carbonyl groups are absolutely
381 conserved in all PoTeMs. This finding is significant becasue it suggests that formation of
382 such iron complexes could be general for all PoTeMs. On the other hand, there is a clear
383 structural diversity among the PoTeM family, which is derived from the polycyclic system
384 (14). While HSAF and alteramides are known for antifungal activity, other members of the
385 PoTeM family exhibit antitumor, antiprotozoal, cytotoxic, and antiviral activities. The
386 structural diversity of PoTeMs may be associated with these activities and may also confer
387 survival advantage to their producers in various habitats. For example, *L. enzymogenes* OH11
388 was originally isolated from the rhizosphere of a pepper plant (32). Whether HSAF and
389 alteramides play a role in plant root colonization is worth a further investigation, as resistance
390 to oxidative stress is important for the survival of bacteria during their interaction with plants.
391 It is not very clear what structural features in these compounds are associated with the
392 antifungal activity, although we found the carbonyl oxygen atoms at C7, C25 and C27 are

393 involved in the iron chelation to form HSAF-Fe complexes. *L. enzymogenes* can produce
394 HSAF and analogs without iron and with iron in the minimal media (up to 500 μM). In reality,
395 it is unlikely that the iron concentration in the natural environment of *L. enzymogenes* would
396 be higher than what we have tested. Several iron chelators have exhibited antifungal activity,
397 such as siderophores produced by *Azospirillum brasilense* could inhibit the growth of
398 *Colletotrichum acutatum* and the siderophore oxachelin from *Streptomyces* sp. GW9/1258
399 showed strong antimicrobial activity against several fungi and Gram-positive bacteria (48,
400 49). Further studies are needed in order to answer whether the antifungal activity and the
401 antioxidant activity are related to each other or exclude each other. Nevertheless, it seems
402 reasonable to assume that the antioxidant activity of HSAF and analogs could enhance the
403 survival rate of the producer microorganism through the enhanced resistance to oxidative
404 stress and thus play a role in plant root colonization during their interaction with plants.
405 Several strategies are evolved in bacteria to modulate the oxidative stress (25-30).

406 In summary, HSAF has been recognized as an antifungal antibiotic with a fascinating
407 chemical structure, new mode of action, and distinct mechanism for biosynthesis (2, 6, 7, 31).
408 Here, we presented evidence to support that HSAF and its analogous compounds may
409 represent a new strategy for microorganisms to modulate the oxidative stress. These
410 "secondary metabolites" confer *L. enzymogenes* to survive in the environment with a high
411 concentration of iron, H_2O_2 or UV radiation. HSAF is the first member of the fast growing
412 PoTeM family of natural products whose potential biological function has been investigated.
413 The genome mining efforts have shown a strikingly conserved organization for PoTeM
414 biosynthetic clusters, which are present in a large number of unexplored genomes of

415 phylogenetically diverse bacteria ranging from proteobacteria to actinomycetes (3, 10, 14).
416 This means there are a large number of new PoTeMs yet to be explored. The understanding
417 the biological function of HSAF shed new lights into the critical role of "secondary
418 metabolites" in the survival of microorganisms in complex ecosystems, and the results will
419 also facilitate the future efforts in new PoTeM exploitation.
420

421 ## MATERIAL AND METHODS
422

423 *Bacterial cultures, primers and PCR*

424 The wild type strain *Lysobacter enzymogenes* OH11 (CGMCC No. 1978) and the HSAF
425 biosynthetic mutant ΔHSAF (Table 1) were cultured in Luria-Bertani (LB) medium (32). For
426 the production of HSAF and its analogs, the strains were cultured in M813 modified medium
427 (4 g Glucose, 3 g K_2HPO_4, 1.2 g NaH_2PO_4, 1 g NH_4Cl, 0.3 g $MgSO_4$, 0.15 g KCl, 10 mg
428 $CaCl_2$, 2.8 mg $FeSO_4 \cdot 7H_2O$, per liter) (50). In the initial experiments, the strains were also
429 cultured in MM2 medium (4 g Glucose, 15 g KH_2PO_4, 34 g Na_2HPO_4, 5.4 g NH_4Cl, 2.5 g
430 NaCl, 0.3 g $MgSO_4$, 10 mg $CaCl_2$, per liter). Table 2 listed the primers used in this study.
431 Phusion High-Fidelity DNA polymerase (Thermo Scientific) was used as the amplification
432 enzyme. The PCR started from an initial denaturation at 98°C for 30 s followed by 30 cycles
433 of amplification (98°C for 10 s, 60°C for 15 s, 72°C for 1 min), and completed with
434 additional 5 min at 72°C. Depending on the DNA templates and primers, the annealing
435 temperature and the elongation time were adjusted in some case
436

437 *Extraction and HPLC analysis of HSAF and its analogs*

438 *L. enzymogenes* OH11 wild type (WT) and HSAF deficiency strain (ΔHSAF), in which a part
439 of *pks-nrps* gene (from +232 bp to +1356 bp with relative to the start codon) of HSAF
440 biosynthetic gene cluster was deleted (32), were incubated into 1 ml LB at 30°C with shaking
441 of 200 rpm for overnight. An aliquot (1%) of the cultures was transferred to 25 ml M813
442 modified (M813m) medium with variable concentrations of $FeSO_4$ (final concentration of 0,
443 1, 10, 100 and 500 μM), 30°C with shaking at 200 rpm for 48 h. The whole cultures (cells
444 and medium) were treated with 75 μl TFA and 25 ml ethyl acetate. The organic phase was
445 dried with the air flow, and the residues were re-dissolved in 200 μl methanol. A 2 μl aliquot
446 of each extract was analyzed by HPLC (Agilent, 1220 Infinity LC). Water/0.05% FA (solvent
447 A) and acetonitrile/0.05% FA (solvent B) were used as the mobile phases with a flow rate of
448 1.0 ml/min. The HPLC program was as follows: 5−25% B in 0−5 min, 25%-80% B in 5−25
449 min, 80−100% B in 25−26 min, maintained to 28 min, back to 5% B at 29 min and
450 maintained to 30 min. HSAF and its analogs were detected at 318 nm on a UV detector. For
451 purification of HSAF, WT was incubated into 10 ml LB at 30°C with shaking at 200 rpm for
452 overnight. An aliquot (1%) of the cell cultures was transferred to 1 L M813m medium and grew
453 at 30°C with shaking at 200 rpm for 48 h. The culture broth was adjusted to pH 2.5 with 37%
454 HCl. The culture was added with the same volume of ethyl acetate, and HSAF was extracted
455 into the organic phase for three times. The ethyl acetate phase was dried using a rotavapor, and
456 HSAF was separated from other metabolites in the extract (850 mg) on a C18 reverse-phase
457 column, eluted with different concentrations of methanol (10%, 30%, 50%, 70%, and 100%).
458 The fraction (552 mg) of 100% methanol was used to purify HSAF (~50 mg) by HPLC.

459

460 *Chelation of HSAF with metal ions*

461 For the chelation with $FeSO_4$, an increased volume (1, 10, 50 µl, in methanol) of the total
462 PoTeM mixture (2 mg/ml) was mixed with 100 µl aqueous solution of $FeSO_4$ (10 mM). For
463 the chelation with other iron salts, the total PoTeM mixture (50 µl, 2 mg/ml) was incubated
464 with 50 µl aqueous solution of $Fe(NH_4)_2(SO_4)_2$, $FeCl_3$, and $Fe(NO_3)_3$ (each 10 mM). For the
465 chelation with other metals, the total PoTeM mixture (50 µl, 0.5 mg/ml) was incubated with
466 50 µl aqueous solution of Na_2SO_4, $MgSO_4$, K_2SO_4, $Ca(NO_3)_2$, $CuSO_4$, and $ZnSO_4$ (each 10
467 mM). Methanol was used as control. For HPLC analysis, the above mixed solutions were
468 dried and then resuspended in 100 µl methanol. A 20 µl aliquot of each of the solutions was
469 analyzed by HPLC (Agilent, 1220 Infinity LC). The HPLC program was as follows:
470 Water/0.05% FA (solvent A) and acetonitrile/0.05% FA (solvent B) were used as the mobile
471 phases with a flow rate of 1.0 ml/min. The program was as follows: 5%-60% B in 0–5 min,
472 60%-100% B in 5–20 min, maintained to 23 min, back to 5% B at 28 min, and maintained to
473 30 min. The metabolites were detected at 230 nm on a UV detector. The experiments were
474 repeated for three times.

475

476 *MS analysis and UV-Visible absorbance spectra of the HSAF-Fe complexes*

477 To prepare the complexes, purified HSAF (20 µl,10 mM) was mixed with an equal volume of
478 each of aqueous $FeSO_4$ (10 mM), $Fe(NH_4)_2(SO_4)_2$ (10 mM), $FeCl_3$ (10 mM), and $Fe(NO_3)_3$
479 (10 mM). Each of the mixtures was dried and re-suspended in 200 µl ddH_2O. Ethyl acetate
480 (200 µl, containing 0.05% TFA) was added to the suspension to extract the HSAF-Fe

complexes, and the organic phase was collected and dried and re-dissolved in 1 ml methanol. A 20 µl aliquot of each of the samples was analyzed by MS and the remaining fraction of the samples was used to determine the UV-visible absorbance spectrum by a spectrophotometer (Shimadzu UV-Vis 2501). After the spectra were taken, 50 µl Na_2EDTA (100 mM, pH 8.0) was added into each of the samples, and the samples were dried and re-suspended in 250 µl ddH_2O. Similar to the above procedure, the HSAF-Fe complexes were extracted with 250 µl ethyl acetate (containing 0.05% TFA), the organic phase was collected and dried and re-dissolved in 1 ml methanol. Then samples then were similarly analyzed by MS and spectrophotometer again. The experiments were repeated for three times.

UV-Visible absorbance titration and association constant determination

To determine the association constant, absorbance spectra were recorded with a spectrophotometer (Shimadzu UV-Vis 2501). The UV-Visible titration assay was performed by using a constant host concentration of HSAF (0.1 mM) and variable concentrations of $Fe(NO_3)_3$ at 25°C. Association constant (K_a) was calcualted using Eq. (4) by applying a nonlinear curve-fitting method (51) on Program of origin 9.0 to changes in absorbance (ΔAbs) at 470 nm.

$$\Delta Abs=(L(1+K_aX+K_aA)-(L^2(K_aX+K_aA+1)^2-4K_a^2AXL^2)^{0.5})/2K_aA \quad (4)$$

Where X and A were the total concentration of the guest and the host, respectively, and L and K_a were treated as parameters. The experiments were repeated for three times.

Assay for deoxyribose degradation

503 This assay was used to determine the antioxidative activity. In the assay, hydroxyl radicals
504 generated by the Fenton reaction would degrade deoxy-D-ribose into malonyldialdehyde
505 (MDA) (35). MDA then would react with 2-thiobarbituric acid to produce a pink pigment,
506 which was determined photometrically at 532 nm (34). To perform the assay, 227.5 µl
507 variable concentration of purified HSAF (final concentration is 0, 5, 10, 20, 40, 80, and 160
508 µM) were added into the reactant mixture containing 45.5 µl Deoxy-D-ribose (52 mM, in 50
509 mM KH_2PO_4, pH 7.4), 91 µl $FeCl_3$ (4 µM, in water), 91 µl KH_2PO_4 buffer (pH 7.4), 45.5 µl
510 H_2O_2 (10 mM, in water), and 45.5 µl ascorbic acid (1 mM, in 50 mM KH_2PO_4, pH 7.4). The
511 samples were mixed and incubated at 30°C for 60 min. After that, 455 µl 2-thiobarbituric acid
512 (1%, in 3% trichloroacetic acid) was added into each of the samples, and the mixtures were
513 incubated at 85°C for 30 min. The supernatant of each of the mixtures was collected
514 following centrifugation (12,000 rpm, 1 min), and the OD_{532} value of the supernatants was
515 determined by spectrophotometer (Shimadzu UV-Vis 2501). The experiments were repeated
516 for three times.
517
518 *Assay for in vitro DNA degradation*
519 The assay followed a previously described method with some modifications (36). The DNA
520 fragments were obtained by PCR using primers listed in Table S2 with a template from the
521 genomic DNA of *L. enzymogenes* OH11, *Lysobacter* 3655, *L. antibioticus* OH13, or *E. coli*.
522 Each of the degradation mixtures contained 100 ng DNA fragment, 20 mM H_2O_2, 150 µM
523 $FeCl_3$ and various concentrations of purified HSAF (0.3125, 0.625, 1.25, 2.5, 5, 10, 20, 40
524 and 80 µM) in 50 mM KH_2PO_4 buffer (pH 7.4). After incubating the mixtures at 37°C for 60

525 min, the samples were applied to 0.8 % agarose gels in TAE buffer. The electrophoresis was
526 performed at 140 V for 15 min, and the bands were visualized in a UV transilluminator
527 (Universal Hood, Bio-Rad). The experiments were repeated for three times.
528
529 *OH11 growth under oxidative stress induced by H_2O_2*
530 WT and ΔHSAF strains were incubated into 1 ml LB at 30°C with shaking of 200 rpm for
531 overnight. A fraction (1%) of the cultures was transferred to 25 ml M813m medium at 30°C
532 with shaking at 200 rpm for 48 h. After the OD_{600} value of each of the cultures was
533 determined, a fraction (1%) of the cultures was added into 25 ml M813m medium containing
534 0, 80, or 800 μM H_2O_2, and the cultures were incubated at 30°C with shaking at 200 rpm for
535 96 h. The OD_{600} values of WT and ΔHSAF strains were recorded every 24 h. The
536 experiments were repeated for three times.
537
538 *Assay for in vitro H_2O_2 degradation*
539 The Hydrogen Peroxide (H_2O_2) Colorimetric Assay Kit (Elabscience, China) was used to
540 detect the concentration of H_2O_2 which could react with ammonium molybdate and produced
541 a yellow complex with the maximum absorption at 405 nm. The reaction system contained 2
542 ml reaction buffer, 100 μl H_2O_2 (60 mM), and 100 μl purified HSAF (4 mM) or 100 μl
543 purified HSAF-Fe complexes (4 mM). Methanol was used as negative control. The reaction
544 system was incubated at 30°C for 30 min, then the OD_{405} value was determined by
545 spectrophotometer.
546

547 *OH11 growth under oxidative stress induced by UV light*

548 For the WT and ΔHSAF of *L. enzymogenes* OH11, the strains were incubated into 1 ml LB at
549 30°C with shaking at 200 rpm for overnight. A fraction (1%) of the cultures was transferred
550 to 25 ml M813m medium at 30°C with shaking at 200 rpm for 48 h. The cultures were
551 adjusted with the medium to the same OD_{600} of 1.5 and a fraction of 10 ml of each of the
552 cultures was spread on a petri dish (9.0 cm, external diameter) and exposed to a UV light
553 source (253.7 nm, Model TUV 30W T8, 102 Volts, 0.37 AMPS, 30 Watts), at a distance of 30
554 cm between the light and the cells for 0 s, 10 s, 30 s or 60 s. For the complementary assay,
555 purified HSAF with a various concentration (final concentration of 0, 20, 80 and 160 μM)
556 was added into the culture of ΔHSAF strain before exposure to UV for 60 s, and methanol
557 was used as control. The cultures were serially diluted and spread on fresh LB plates. The
558 numbers of colonies on each plate were counted after 72 h of incubation at 30°C. The
559 experiments were repeated for three times.

560

561 *ROS detection*

562 The production of ROS in WT and ΔHSAF strains were detected using a previous method
563 with some modifications (38). WT and ΔHSAF strains were incubated into 1 ml LB, 30°C
564 with shaking of 200 rpm for overnight. A fraction (1%) of the cultures was transferred into 25
565 ml M813m medium with various concentrations of $FeSO_4$ (0, 10, 500 μM). After 72 h of
566 growth, the cultures were diluted 30-fold with the same medium in a 96-well plate. Then
567 H2DCFDA was added to the wells with a final concentration of 10 μM. The incubation of the
568 plate continued in the dark at 30°C with shaking at 60 rpm for 6 h. Fluorescence was

measured in a BioTek Synergy H1 plate reader (excitation, 495 nm; emission, 527 nm). In addition, the cultures of WT and ΔHSAF from regular M813m medium containing 10 μM $FeSO_4$ were treated with UV for 60 s without or with purified HSAF (final concentration 160 μM), or treated with H_2O_2 (final concentration 40 mM) before fluorescence detection. The experiments were repeated for three times.

Assay for ROS scavenging activity of HSAF and HSAF-Fe complexes

HSAF and HSAF-Fe complexes were tested for *in vitro* ROS scavenging activity using DPPH (2,2-Diphenyl-1-picrylhydrazyl) which is a stable radical and has the maximum absorption at 520 nm. In reaction system, 1 ml DPPH (5 mg/ml, dissolved in ethanol) was mixed with 200 μl various concentration of purified HSAF or HSAF-Fe complexes (final concentration was 0 μM, 20 μM, 40 μM, 80 μM and 160 μM, dissolved in ethanol), and then incubated at room temperature for 0.5 h, 24 h, 72 h and 120 h. The OD_{520} value of samples was determined by spectrophotometer, which was used to calculate the remaining DPPH, by following the formula: DPPH (%) = $A/A_0*100\%$, A_0 represents the OD_{520} value of 0 μM. Ascorbic acid was used as positive control and the OD_{520} value was determined immediately.

Extraction of the HSAF-Fe complexes in vivo

WT was incubated into 1 ml LB, 30°C with shaking at 200 rpm for overnight. A fraction (1%) of the cultures was transferred into 50 ml M813m medium containing 500 μM $FeSO_4$, and incubated at 30°C with shaking at 200 rpm for 48 h. After centrifugation (12,000 rpm, 5 min), the precipitate presented as two layers, and the upper layer was collected and extracted with

50 ml ethyl acetate (containing 0.3% TFA). The organic phase was dried and re-dissolved in 200 µl methanol. The methanol solutions were used for MS analysis. The experiments were repeated three times.

Molecular mechanical and quantum mechanical calculations

The calculations were performed with the quantum chemistry polarizable force field (QuanPol) (52) program and the General Atomic and Molecular Electronic Structure System [GAMESS (53, 54)] package. The MMFF94 force field (55-58) was used in the global search of the most stable molecular structures. In the global search, one million steps (time step size = 1 fs) of molecular dynamic simulation were performed at 700 K, with a geometry optimization at every 1000 steps. Using the MMFF94 identified minimum structures, quantum mechanical density functional theory method B3LYP (59, 60) [with Grimme's empirical dispersion correction version III (61)] was used to refine the molecular geometries. The 6-31G* basis set (62) was used.

ACKNOWLEDGEMENTS

This work was supported in part by NSFC (31872018), University of Nebraska Collaboration Initiative Seed Grant, and the Nebraska Public Power District through the Nebraska Center for Energy Sciences Research at the University of Nebraska-Lincoln. L.Y. was supported by a postdoctoral fellowship from Jiangsu Academy of Agricultural Sciences. The calculations were performed with resources at the University of Nebraska-Lincoln Holland Computing Center.

613

614 **Conflict of Interest:** the authors have no conflict of interest to declare.

615

616

617 **REFERENCES**

618

619 1. Jomon K, Kuroda Y, Ajisaka M, Sakai H. 1972. A new antibiotic, ikarugamycin. J
620 Antibiot (Tokyo) 25:271-280.
621 2. Yu F, Zaleta-Rivera K, Zhu X, Huffman J, Millet JC, Harris SD, Yuen G, Li XC, Du L.
622 2007. Structure and biosynthesis of heat-stable antifungal factor (HSAF), a broad-spectrum
623 antimycotic with a novel mode of action. Antimicrob Agents Chemother 51:64-72.
624 3. Blodgett JA, Oh DC, Cao S, Currie CR, Kolter R, Clardy J. 2010. Common biosynthetic
625 origins for polycyclic tetramate macrolactams from phylogenetically diverse bacteria. Proc
626 Natl Acad Sci U S A 107:11692-11697.
627 4. Qi Y, Ding E, Blodgett JAV. 2018. Native and engineered clifednamide biosynthesis in
628 multiple *Streptomyces* spp. ACS Synth Biol 7:357-362.
629 5. Saha S, Zhang W, Zhang G, Zhu Y, Chen Y, Liu W, Yuan C, Zhang Q, Zhang H, Zhang L,
630 Zhang W, Zhang C. 2017. Activation and characterization of a cryptic gene cluster reveals a
631 cyclization cascade for polycyclic tetramate macrolactams. Chem Sci 8:1607-1612.
632 6. Ding Y, Li Y, Li Z, Zhang J, Lu C, Wang H, Shen Y, Du L. 2016. Alteramide B is a
633 microtubule antagonist of inhibiting *Candida albicans*. Biochim Biophys Acta
634 1860:2097-2106.
635 7. Ding Y, Li Z, Li Y, Lu C, Wang H, Shen Y, Du L. 2016. HSAF-induced antifungal effects
636 in *Candida albicans* through ROS-mediated apoptosis. RSC Adv 6:30895-30904.
637 8. Yu HL, Jiang SH, Bu XL, Wang JH, Weng JY, Yang XM, He KY, Zhang ZG, Ao P, Xu J,
638 Xu MJ. 2017. Structural diversity of anti-pancreatic cancer capsimycins identified in

639 mangrove-derived *Streptomyces xiamenensis* 318 and post-modification via a novel
640 cytochrome P450 monooxygenase. Sci Rep 7:40689.
641 9. Cao S, Blodgett JA, Clardy J. 2010. Targeted discovery of polycyclic tetramate
642 macrolactams from an environmental *Streptomyces* strain. Org Lett 12:4652-4654.
643 10. Liu Y, Wang H, Song R, Chen J, Li T, Li Y, Du L, Shen Y. 2018. Targeted discovery and
644 combinatorial biosynthesis of polycyclic tetramate macrolactam combamides A-E. Org Lett
645 20:3504-3508.
646 11. Lou L, Qian G, Xie Y, Hang J, Chen H, Zaleta-Rivera K, Li Y, Shen Y, Dussault PH, Liu
647 F, Du L. 2011. Biosynthesis of HSAF, a tetramic acid-containing macrolactam from
648 *Lysobacter enzymogenes*. J Am Chem Soc 133:643-645.
649 12. Li Y, Chen H, Ding Y, Xie Y, Wang H, Cerny RL, Shen Y, Du L. 2014. Iterative assembly
650 of two separate polyketide chains by the same single-module bacterial polyketide synthase in
651 the biosynthesis of HSAF. Angew Chem Int Ed Engl 53:7524-7530.
652 13. Xu L, Wu P, Wright SJ, Du L, Wei X. 2015. Bioactive polycyclic tetramate macrolactams
653 from *Lysobacter enzymogenes* and their absolute configurations by theoretical ECD
654 calculations. J Nat Prod 78:1841-1847.
655 14. Li Y, Wang H, Liu Y, Jiao Y, Li S, Shen Y, Du L. 2018. Biosynthesis of the polycyclic
656 system in the antifungal HSAF and analogues from *Lysobacter enzymogenes*. Angew Chem
657 Int Ed Engl 57:6221-6225.
658 15. Xie Y, Wright S, Shen Y, Du L. 2012. Bioactive natural products from *Lysobacter*. Nat
659 Prod Rep 19:1277-1287.
660 16. Jakobi M, Winkelmann G, Kaiser D, Kempter C, Jung G, Berg G, Bahl H. 1996.

661 Maltophilin: A new antifungal compound produced by *Stenotrophomonas maltophilia* R3089.
662 J Antibiot 49:1101-1104.
663 17. Hashidoko Y, Nakayama T, Homma Y, Tahara S. 1999. Structure elucidation of
664 xanthobaccin A, a new antibiotic produced from *Stenotrophomonas* sp strain SB-K88.
665 Tetrahed Lett 40:2957-2960.
666 18. Gunasekera SP, Gunasekera M, Mccarthy P. 1991. Discodermide - a new bioactive
667 macrocyclic lactam from the marine sponge *Discodermia-Dissoluta*. J Org Chem
668 56:4830-4833.
669 19. Kanazawa S, Fusetani N, Matsunaga S. 1993. Cylindramide - cytotoxic tetramic acid
670 lactam from the marine sponge *Halichondria-Cylindrata* Tanita and Hoshino. Tetrahed Lett
671 34:1065-1068.
672 20. Hoshino S, Wong CP, Ozeki M, Zhang HP, Hayashi F, Awakawa T, Asamizu S, Onaka H,
673 Abe I. 2018. Umezawamides, new bioactive polycyclic tetramate macrolactams isolated from
674 a combined-culture of *Umezawaea* sp and mycolic acid-containing bacterium. J Antibiot
675 71:653-657.
676 21. Antosch J, Schaefers F, Gulder TA. 2014. Heterologous reconstitution of ikarugamycin
677 biosynthesis in *E. coli*. Angew Chem Int Ed Engl 53:3011-3014.
678 22. Zhang G, Zhang W, Zhang Q, Shi T, Ma L, Zhu Y, Li S, Zhang H, Zhao YL, Shi R,
679 Zhang C. 2014. Mechanistic insights into polycycle formation by reductive cyclization in
680 ikarugamycin biosynthesis. Angew Chem Int Ed Engl 53:4840-4844.
681 23. Greunke C, Glöckle A, Antosch J, Gulder TAM. 2017. Biocatalytic total synthesis of
682 ikarugamycin. Angew Chem Int Ed Engl 56:4351-4355.

683 24. Davies J. 2006. Are antibiotics naturally antibiotics? J Industr Microbiol Biotech
684 33:496-499.
685 25. Lu J, Holmgren A. 2014. The thioredoxin antioxidant system. Free Radical Biol Med
686 66:75-87.
687 26. King KY, Horenstein JA, Caparon MG. 2000. Aerotolerance and peroxide resistance in
688 peroxidase and PerR mutants of *Streptococcus pyogenes*. J Bacteriol 182:5290-5299.
689 27. Stahl W, Sies H. 2003. Antioxidant activity of carotenoids. Mol Aspect Med 24:345-351.
690 28. Schoner TA, Gassel S, Osawa A, Tobias NJ, Okuno Y, Sakakibara Y, Shindo K,
691 Sandmann G, Bode HB. 2016. Aryl polyenes, a highly abundant class of bacterial natural
692 products, are functionally related to antioxidative carotenoids. ChemBioChem 17:247-253.
693 29. Wang Y, Qian G, Li Y, Wright S, Shen Y, Liu F, Du L. 2013. Biosynthetic mechanism for
694 sunscreens of the biocontrol agent *Lysobacter enzymogenes*. PLoS One 8:e66633.
695 30. Mironov A, Seregina T, Nagornykh M, Luhachack LG, Korolkova N, Lopes LE, Kotova
696 V, Zavilgelsky G, Shakulov R, Shatalin K, Nudler E. 2017. Mechanism of H_2S-mediated
697 protection against oxidative stress in *Escherichia coli*. Proc Nat Acad Sci U S A
698 114:6022-6027.
699 31. Li S, Du L, Yuen G, Harris SD. 2006. Distinct ceramide synthases regulate polarized
700 growth in the filamentous fungus *Aspergillus nidulans*. Mol Biol Cell 17:1218-1227.
701 32. Wang Y, Zhao Y, Zhang J, Zhao Y, Shen Y, Su Z, Xu G, Du L, Huffman JM, Venturi V,
702 Qian G, Liu F. 2014. Transcriptomic analysis reveals new regulatory roles of Clp signaling in
703 secondary metabolite biosynthesis and surface motility in *Lysobacter enzymogenes* OH11.
704 Appl Microbiol Biotechnol 98:9009-9020.

705 33. Khan A, Singh P, Srivastava A. 2018. Synthesis, nature and utility of universal iron
706 chelator - Siderophore: A review. Microbiol Res 212:103-111.
707 34. Chobot V, Hadacek F, Kubicova L. 2014. Effects of selected dietary secondary
708 metabolites on reactive oxygen species production caused by iron(II) autoxidation. Molecules
709 19:20023-20033.
710 35. Chobot V. 2010. Simultaneous detection of pro- and antioxidative effects in the variants
711 of the deoxyribose degradation assay. J Agr Food Chem 58:2088-2094.
712 36. Zhao CY, Dodin G, Yuan CS, Chen HF, Zheng RL, Jia ZJ, Fan BT. 2005. "In vitro"
713 protection of DNA from Fenton reaction by plant polyphenol verbascoside. Biochim Biophys
714 Acta-Gen Subj 1723:114-123.
715 37. Kimeswenger S, Schwarz A, Fodinger D, Muller S, Pehamberger H, Schwarz T,
716 Jantschitsch C. 2016. Infrared A radiation promotes survival of human melanocytes carrying
717 ultraviolet radiation-induced DNA damage. Exp Dermatol 25:447-452.
718 38. Maynard A, Butler NL, Ito T, da Silva AJ, Murai M, Chen T, Koffas MAG, Miyoshi H,
719 Barquera B. 2019. Antibiotic korormicin A kills bacteria by producing reactive oxygen
720 species. J Bacteriol 201: e00718-18.
721 39. Bredenbruch F, Geffers R, Nimtz M, Buer J, Haussler S. 2006. The *Pseudomonas*
722 *aeruginosa* quinolone signal (PQS) has an iron-chelating activity. Environ Microbiol
723 8:1318-1329.
724 40. Santos AL, Oliveira V, Baptista I, Henriques I, Gomes NCM, Almeida A, Correia A,
725 Cunha A. 2013. Wavelength dependence of biological damage induced by UV radiation on
726 bacteria. Arch Microbiol 195:63-74.

727 41. Halliwell B, Aeschbach R, Loliger J, Aruoma OI. 1995. The characterization of
728 antioxidants. Food Chem Toxicol 33:601-617.
729 42. Hadacek F, Bachmann G, Engelmeier D, Chobot V. 2011. Hormesis and a chemical
730 raison d'etre for secondary plant metabolites. Dose-Response 9:79-116.
731 43. Macomber L, Rensing C, Imlay JA. 2007. Intracellular copper does not catalyze the
732 formation of oxidative DNA damage in *Escherichia coli*. J Bacteriol 189:1616-1626.
733 44. Mello AC, Meneghini R. 1991. Iron is the intracellular metal involved in the production
734 of DNA damage by oxygen radicals. Mutat Res 251:109-113.
735 45. Mello AC, Meneghini R. 1984. In vivo formation of single-strand breaks in DNA by
736 hydrogen-peroxide is mediated by the Haber-Weiss Reaction. Biochim Biophys Acta
737 781:56-63.
738 46. Imlay JA. 2013. The molecular mechanisms and physiological consequences of oxidative
739 stress: lessons from a model bacterium. Nat Rev Microbiol 11:443-454.
740 47. De Laat J, Gallard H. 1999. Catalytic decomposition of hydrogen peroxide by Fe(III) in
741 homogeneous aqueous solution: Mechanism and kinetic modeling. Environ Sci Technol
742 33:2726-2732.
743 48. Sontag B, Gerlitz M, Paululat T, Rasser HF, Grun-Wollny I, Hansske FG. 2006.
744 Oxachelin, a novel iron chelator and antifungal agent from *Streptomyces* sp GW9/1258. J
745 Antibiot 59:659-663.
746 49. Tortora ML, Diaz-Ricci JC, Pedraza RO. 2011. *Azospirillum brasilense* siderophores
747 with antifungal activity against *Colletotrichum acutatum*. Archives of Microbiology
748 193:275-286.

749 50. Palumbo JD, Sullivan RF, Kobayashi DY. 2003. Molecular characterization and
750 expression in *Escherichia coli* of three beta-1,3-glucanase genes from *Lysobacter*
751 *enzymogenes* strain N4-7. J Bacteriol 185:4362-4370.
752 51. Li WS, Jiang DL, Suna Y, Aida T. 2005. Cooperativity in chiroptical sensing with
753 dendritic zinc porphyrins. J Am Chem Soc 127:7700-7702.
754 52. Thellamurege NM, Si D, Cui F, Zhu H, Lai R, Li H. 2013. QuanPol: A full spectrum and
755 seamless QM/MM program. J Comput Chem 34:2816-2833.
756 53. Schmidt MW, Baldridge KK, Boatz JA, Elbert ST, Gordon MS, Jensen JH, Koseki S,
757 Matsunaga N, Nguyen KA, Su SJ, Windus TL, Dupuis M, Montgomery JA. 1993. General
758 atomic and molecular electronic-structure system. J Comput Chem 14:1347-1363.
759 54. Gordon MS, Schmidt MW. 2005. Advances in electronic structure theory: GAMESS a
760 decade later. *In* Dykstra CE, Frenking G, Kim KS, Scuseria GE (ed), Theory and
761 Applications of Computational Chemistry. Elsevier.
762 55. Halgren TA, Nachbar RB. 1996. Merck molecular force field. IV. conformational
763 energies and geometries for MMFF94. J Comput Chem 17:587-615.
764 56. Halgren TA. 1996. Merck molecular force field. II. MMFF94 van der Waals and
765 electrostatic parameters for intermolecular interactions. J Comput Chem 17:520-552.
766 57. Halgren TA. 1996. Merck molecular force field. III. Molecular geometries and
767 vibrational frequencies for MMFF94. J Comput Chem 17:553-586.
768 58. Halgren TA. 1996. Merck molecular force field. V. Extension of MMFF94 using
769 experimental data, additional computational data, and empirical rules. J Comput Chem
770 17:616-641.

771 59. Becke AD. 1993. Density - functional thermochemistry. III. The role of exact exchange.
772 J Chem Phys 98:5648-5652.
773 60. Hertwig RH, Koch W. 1997. On the parameterization of the local correlation functional.
774 What is Becke-3-LYP? Chem Phys Lett 268:345-351.
775 61. Grimme S, Antony J, Ehrlich S, Krieg H. 2010. A consistent and accurate ab initio
776 parametrization of density functional dispersion correction (DFT-D) for the 94 elements H-Pu.
777 J Chem Phys 132:154104.
778 62. Francl MM, Pietro WJ, Hehre WJ, Binkley JS, Gordon MS, Defrees DJ, Pople JA. 1982.
779 Self-Consistent Molecular-Orbital Methods .23. A Polarization-Type Basis Set for 2nd-Row
780 Elements. J Chem Phys 77:3654-3665.
781
782

783 **Table 1.** Bacterial strains used in this study.

784

Bacterial strains	Relevant characteristics[a]	Source/reference
Lysobacter		
L. enzymogenes OH11	Wild-type, Kan^r	CGMCC No. 1978
ΔHSAF	HSAF deficiency strain	(32)

785 [a]Kan^r, kanamycin resistant.

786

787 **Table 2.** Primers used in this study.

788

Primers	Sequence(5'-3')
OH11-F	CGGGGCCCCATTGGAACGACAGCCTCTT
OH11-R	CCGCTCGAGCGGCAAGACAGGGGAAGA
3655-F	CGGGGCCCTTTGGTTGTTCCATCCGA
3655-R	CGGGATCCATCGAGGAGCACGGCATC
OH13-F	CTGCAGGACTTCGAACACA
OH13-R	GATTGACTCCTTGGTGCTC
E-F	ATAACGGAGAACGGAATCG
E-R	ACGCATTACTATCTGACCAA

789

790

791

792

793

794 **Figure Legends**

795

796 **Figure 1**. Chemical structure of HSAF and analogs (alteramides) isolated from *Lysobacter*
797 *enzymogenes*.

798 **Figure 2.** Formation of PoTeM-Fe complexes. a) Appearance of cultures of *L. enzymogenes*
799 OH11 wild type (WT) and HSAF non-producer mutant (ΔHSAF) grown in M813m medium
800 containing a different concentration of $FeSO_4$. b) Appearance of the total crude extract of
801 PoTeM (200 µl) from cultures (25 ml) of WT and ΔHSAF grown in M813m containing a
802 different concentration of $FeSO_4$. c) Color change in the solution of $FeSO_4$ (10 mM, 100 µl)
803 when added with the total crude extract of PoTeM (1-50 µl, 2 µg/µl) from WT cultured in
804 M813m containing 10 µM $FeSO_4$, with methanol as negative control. I, positive control
805 (crude extract of PoTeM from WT grown in M813m containing 500 µM $FeSO_4$). d) Color
806 change in the solution of various iron salts (10 mM, 50 µl), without (0) or with 50 µl
807 methanol (II) or with 50 µl (2 µg/µl) of the total crude extract of PoTeM (III). e) HPLC
808 analysis of the isolated PoTeMs, with or without iron salts added.

809 **Figure 3.** MS analysis of the products of HSAF with $FeSO_4$ (a), $Fe(NH_4)_2(SO_4)_2$ (b), $FeCl_3$ (c)
810 and $Fe(NO_3)_3$ (d), in absence or presence of the metal chelator EDTA. Standard HSAF gave
811 *m/z* 513 for $[HSAF+H]^+$ and *m/z* 1025 for $[2HSAF+H]^+$). In the mixtures of HSAF and iron
812 salts, the peak at *m/z* 1079 was coincident with $[2HSAF-H+Fe]^+$, whereas the peak at *m/z*
813 1591 was coincident with $[3HSAF-H+Fe]^+$.

814 **Figure 4.** The *in vitro* antioxidant activity and the *in vivo* protective effect of HSAF for *L.*
815 *enzymogenes* grown in the presence of H_2O_2. a) *In vitro* deoxy-D-ribose degradation assay for

816 the antioxidant activity of HSAF. The activity is presented as thiobarbituric acid reactive
817 species (TBARS) levels relative to the control (100% = TBARS of the control reaction
818 mixture without HSAF). b) *In vitro* assay of the Fenton reaction-caused DNA fragment
819 degradation and the protective effect of HSAF. c-e) *In vivo* H_2O_2 sensitive assay of the WT
820 and ΔHSAF strains cultured in M813m medium containing 0 (c), 80 (d) , or 800 μM (e) H_2O_2,
821 and the OD_{600} value was determined every 24 h. Data are presented as averages of three
822 independent experiments each conducted in triplicate. *, $P < 0.05$; **, $P < 0.01$.

823 **Figure 5.** The protective effect of HSAF for *L. enzymogenes* exposed to UV light and ROS
824 level in *L. enzymogenes* under oxidative stress. a) The WT and ΔHSAF strains were exposed
825 to UV light for 0, 10, 30, and 60 s, and the numbers of colonies on each plate were counted
826 after 72 h of incubation at 30°C. b) Rescue of the UV-light sensitivity of ΔHSAF strain by
827 exogenous HSAF. ΔHSAF strain was added with a variable amount of HSAF (0, 20, 80, 160
828 μM) and then exposed to UV light for 60 s. c) ROS level in the WT and ΔHSAF strains
829 cultured in different media. No Fe, M813 minimal medium without $FeSO_4$; M813m, M813
830 modified medium containing 10 μM $FeSO_4$; High Fe, M813 modified medium containing
831 500 μM $FeSO_4$. d) ROS level in the WT and ΔHSAF strains treated with 40 mM H_2O_2. e)
832 ROS level in the WT and ΔHSAF strains treated with UV light for 60 s. Methanol was used
833 as control. Data are presented as averages of three independent experiments each conducted
834 in triplicate. *, $P < 0.05$; **, $P < 0.01$.

835 **Figure 6.** Molecular structure of HSAF-Fe complexes obtained from the molecular
836 mechanical force field method and quantum mechanical method. Two molecules (a) or three
837 molecules (b) of HSAF can chelate one iron ion.

838 **Figure 1.**

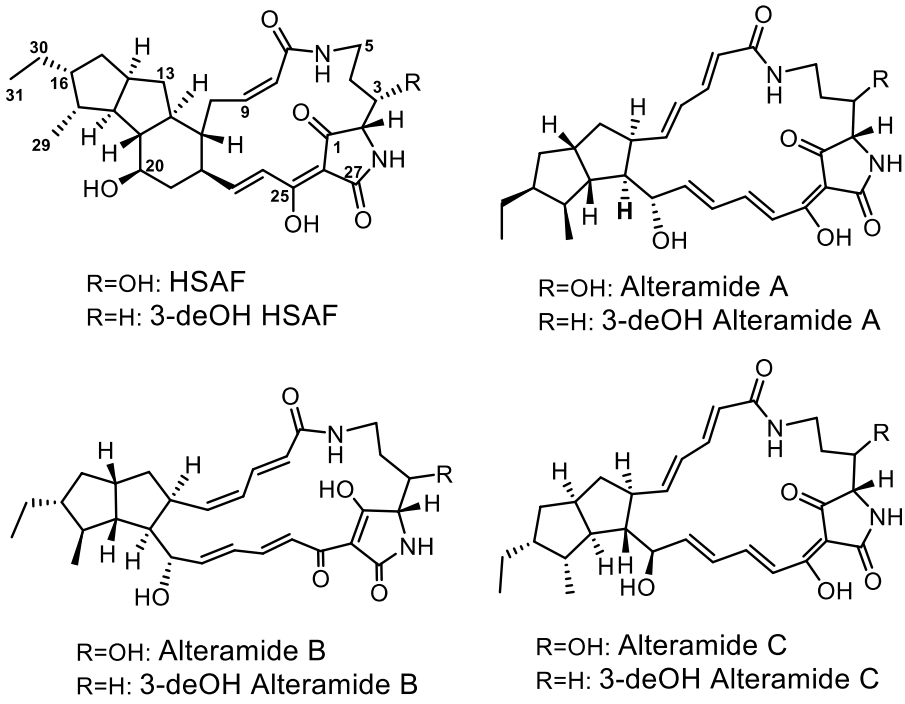

839

840

841 **Figure 1.** Chemical structure of HSAF and analogs (alteramides) isolated from *Lysobacter*

842 *enzymogenes*.

843

844

845

846

847 **Figure 2.**

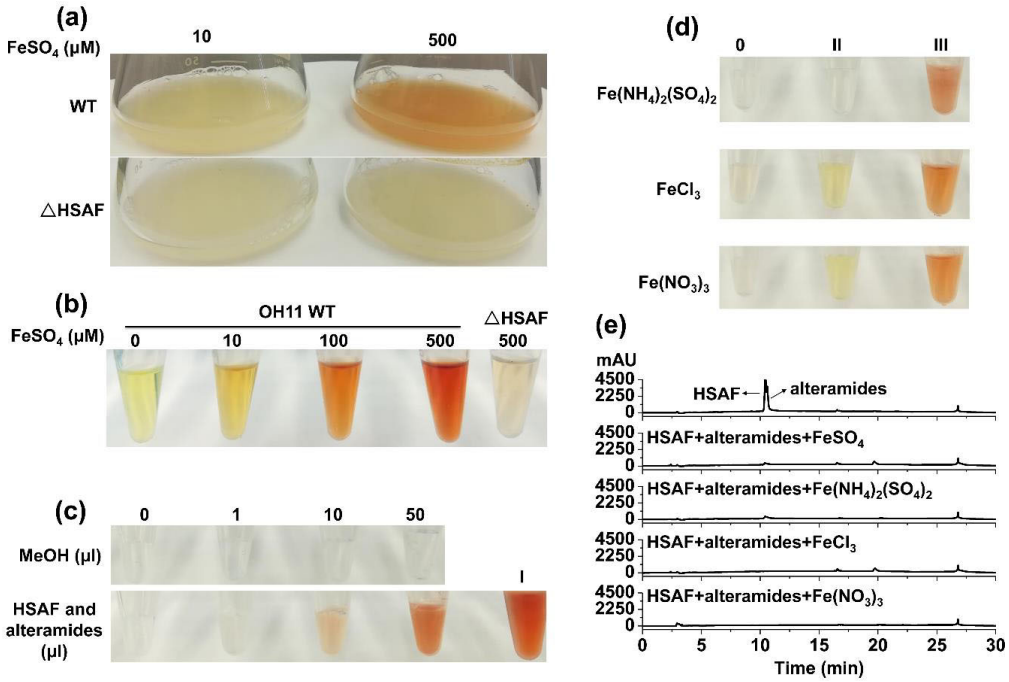

848

849 **Figure 2.** Formation of PoTeM-Fe complexes. a) Appearance of cultures of *L. enzymogenes*
850 OH11 wild type (WT) and HSAF non-producer mutant (ΔHSAF) grown in M813m medium
851 containing a different concentration of $FeSO_4$. b) Appearance of the total crude extract of
852 PoTeM (200 μl) from cultures (25 ml) of WT and ΔHSAF grown in M813m containing a
853 different concentration of $FeSO_4$. c) Color change in the solution of $FeSO_4$ (10 mM, 100 μl)
854 when added with the total crude extract of PoTeM (1-50 μl, 2 μg/μl) from WT cultured in
855 M813m containing 10 μM $FeSO_4$, with methanol as negative control. I, positive control
856 (crude extract of PoTeM from the WT grown in M813m containing 500 μM $FeSO_4$). d) Color
857 change in the solution of various iron salts (10 mM, 50 μl), without (0) or with 50 μl
858 methanol (II) or with 50 μl (2 μg/μl) of the total crude extract of PoTeM (III). e) HPLC
859 analysis of the isolated PoTeMs, with or without iron salts added.

Figure 3.

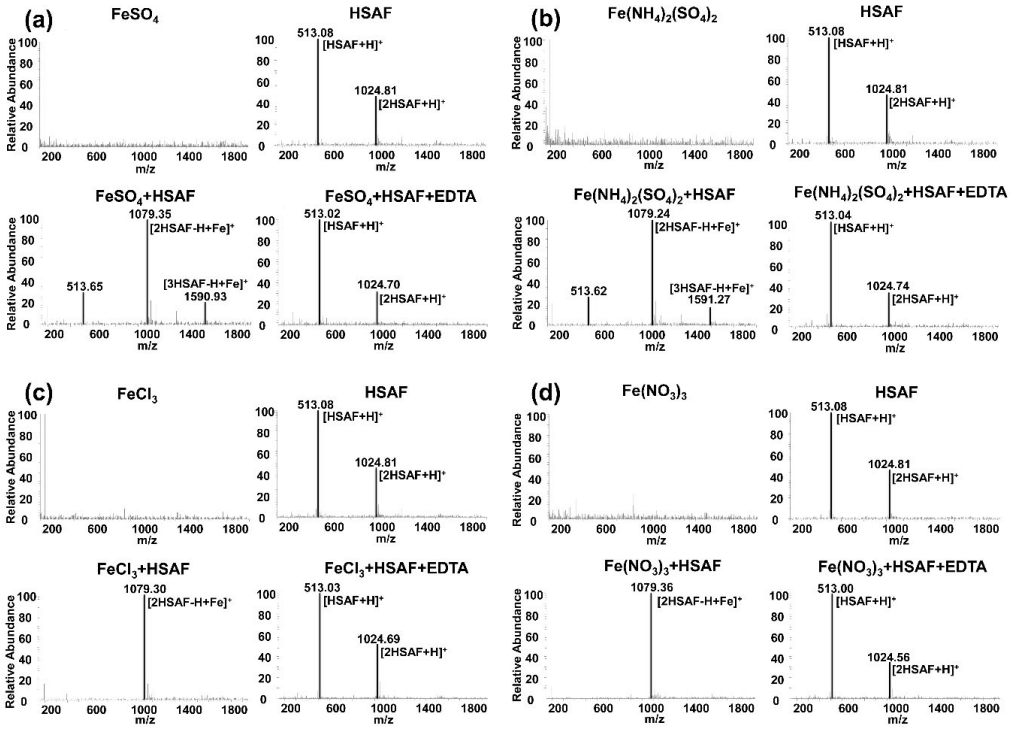

Figure 3. MS analysis of the products of HSAF with $FeSO_4$ (a), $Fe(NH_4)_2(SO_4)_2$ (b), $FeCl_3$ (c) and $Fe(NO_3)_3$ (d), in absence or presence of the metal chelator EDTA. Standard HSAF gave *m/z* 513 for $[HSAF+H]^+$ and *m/z* 1025 for $[2HSAF+H]^+$). In the mixtures of HSAF and iron salts, the peak at *m/z* 1079 was coincident with $[2HSAF-H+Fe]^+$, whereas the peak at *m/z* 1591 was coincident with $[3HSAF-H+Fe]^+$.

Figure 4.

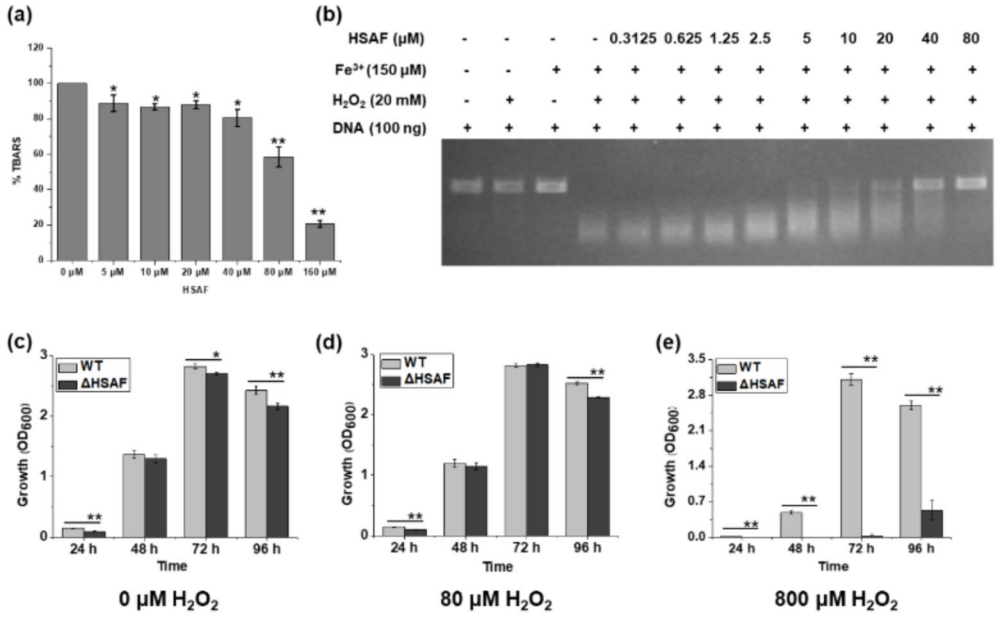

Figure 4. The *in vitro* antioxidant activity and the *in vivo* protective effect of HSAF for *L. enzymogenes* grown in the presence of H_2O_2. a) *In vitro* deoxy-D-ribose degradation assay for the antioxidative activity of HSAF. The activity is presented as thiobarbituric acid reactive species (TBARS) levels relative to the control (100% = TBARS of the control reaction mixture without HSAF). b) *In vitro* assay of the Fenton reaction-caused DNA fragment degradation and the protective effect of HSAF. c-e) *In vivo* H_2O_2 sensitive assay of the WT and ΔHSAF strains cultured in M813m medium containing 0 (c), 80 (d) , or 800 μM (e) H_2O_2, and the OD_{600} value was determined every 24 h. Data are presented as averages of three independent experiments each conducted in triplicate. *, $P < 0.05$; **, $P < 0.01$.

889 **Figure 5**

890

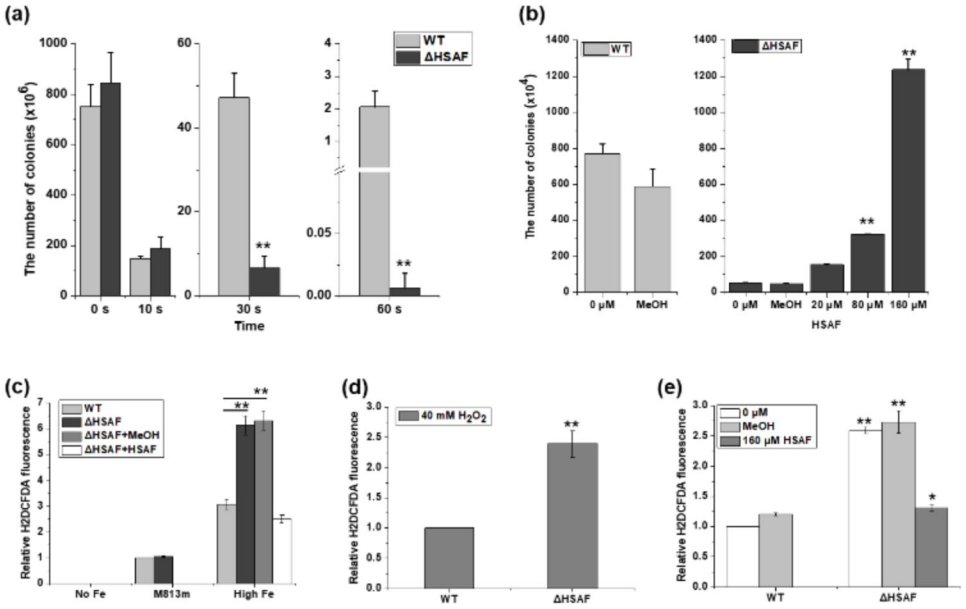

891

892

893 **Figure 5.** The protective effect of HSAF for *L. enzymogenes* exposed to UV light and ROS

894 level in *L. enzymogenes* under oxidative stress. a) The WT and ΔHSAF strains were exposed

895 to UV light for 0, 10, 30, and 60 s, and the numbers of colonies on each plate were counted

896 after 72 h of incubation at 30°C. b) Rescue of the UV-light sensitivity of ΔHSAF strain by

897 exogenous HSAF. ΔHSAF strain was added with a variable amount of HSAF (0, 20, 80, 160

898 μM) and then exposed to UV light for 60 s. c) ROS level in the WT and ΔHSAF strains

899 cultured in different media. No Fe, M813 minimal medium without $FeSO_4$; M813m, M813

900 modified medium containing 10 μM $FeSO_4$; High Fe, M813 modified medium containing

901 500 μM $FeSO_4$. d) ROS level in the WT and ΔHSAF strains treated with 40 mM H_2O_2. e)

902 ROS level in the WT and ΔHSAF strains treated with UV light for 60 s. Methanol was used

903 as control. Data are presented as averages of three independent experiments each conducted

904 in triplicate. *, $P < 0.05$; **, $P < 0.01$.

905 **Figure 6.**

906 a)

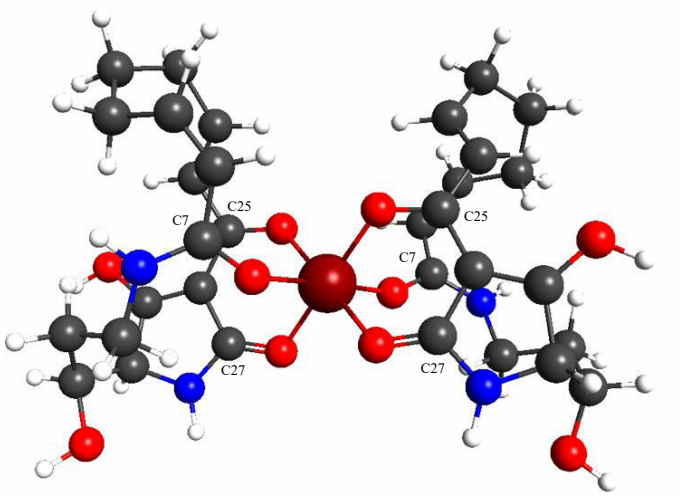

907

908 b)

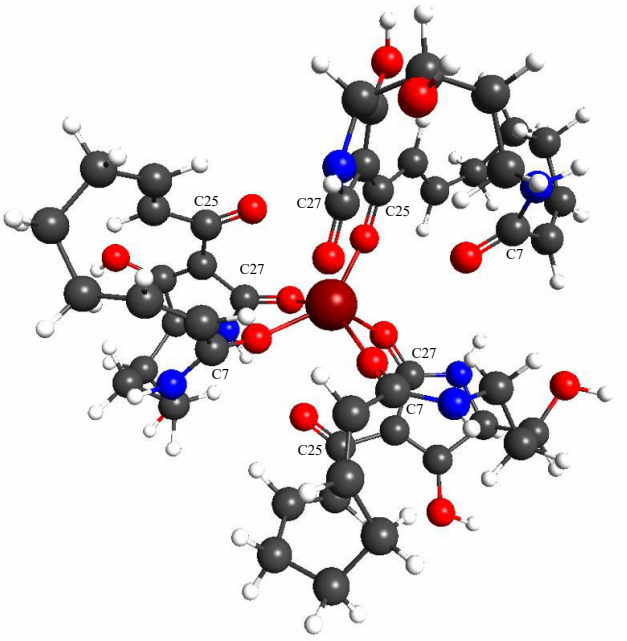

909

910 **Figure 6.** Molecular structure of HSAF-Fe complexes obtained from the molecular

911 mechanical force field method and quantum mechanical method. Two molecules (a) or three

912 molecules (b) of HSAF can chelate one iron ion.